Quantum Electronics **51** (5) 366–370 (2021)

https://doi.org/10.1070/QEL17534

Luminescent properties of a ZnO whisker array as a scintillation detector material

A.P. Tarasov, I.D. Venevtsev, A.E. Muslimov, L.A. Zadorozhnaya, P.A. Rodnyi, V.M. Kanevsky

Abstract. **We have studied luminescent properties of a ZnO whisker array, a promising crystalline material for scintillation detectors, capable of ensuring a fast and strong response and a short afterglow time. Measurements have been performed under X-ray and UV optical excitation. We present a comparative analysis of spectral features of the near-band-edge emission of the whisker array at low (~80 K) and room temperatures in relation to the excitation method.**

Keywords: *ZnO, whiskers, scintillators, X-ray luminescence, photoluminescence, near-band-edge emission, cryogenic temperatures, A-band.*

1. Introduction

Zinc oxide (ZnO) is a well-known wide band gap semiconductor which finds application in many areas and has a considerable potential for extending its application field [1, 2]. One rapidly evolving use of ZnO is related to scintillation detection. Scintillators based on ZnO structures have a rather wide application area for detecting various types of ionising radiation, including high-energy physics, industrial tomography, and noninvasive medical diagnosis based on computed and positron emission tomography techniques [3–8]. The key advantages of ZnO include a subnanosecond decay time and a band gap (~3.3 eV at room temperature) which is narrower than those of most analogues [9, 10], with a potentially strong scintillation response [9]. Also important is the technological aspect: at present, ZnO-based scintillators can be made in a variety of forms (ceramics, films, tetrapods, nanopowders, nanorod and whisker arrays, and others). Besides, the use of ZnO nano- and microstructures is thought to be able to ensure not only a fast X-ray response but also high spatial resolution [11–13]. At the same time, understanding the mechanisms of X-ray luminescence (XRL) in ZnO structures is important for the ability to improve the performance of such scintillators. In particular, since a key role in scintillation detection is played by a fast luminescence component, it is of interest to identify the nature of the near-band-edge (NBE) emission under X-ray excitation.

XRL spectra are difficult to interpret directly because of the poor variability of XRL spectroscopy in choosing luminescence excitation and observation conditions. At the same time, UV photoluminescence spectroscopy is easier to implement and more flexible, which allows one to carry out a more detailed study and, as a consequence, obtain a larger data set for analysis. However, since the mechanisms underlying the interaction of UV photons and X-rays with ZnO differ drastically, it is not yet fully clear to what extent the results of luminescence measurements by these methods are comparable and, specifically, in what cases and under what conditions photoluminescence spectroscopy can be used in analysis of XRL spectra. In our opinion, this issue has not yet been addressed in sufficient detail in the literature. Moreover, in the few studies concerned with photoluminescence and XRL spectra of ZnO structures (see e.g. Refs [14, 15]), distinctions between such spectra are usually rather strong, confirming that this is a topical issue.

In this paper, we present a comparative analysis of the XRL and photoluminescent properties of a ZnO whisker array at cryogenic (~80 K) and room temperatures, with emphasis on interpretation of NBE emission, and a preliminary evaluation of the correctness of comparison of results obtained with the use of two distinct excitation methods with application to the ZnO structure under study.

2. Samples and characterisation techniques

Wurtzite ZnO whisker arrays were grown by chemical vapour deposition [16]. Oxygen concentration in the oxygen–argon flow used did not exceed 10%. The temperature in the evaporation zone was 650 °C and that in the growth zone was 580 °C. As substrates, we used single-crystal sapphire plates 10×10 mm in dimensions.

Microscopic examination was carried out on a JEOL NeoScope 2 (JCM-6000) scanning electron microscope. The average whisker length was determined by examining a cross section of a specimen by electron microscopy.

X-ray luminescence was excited by continuous radiation from a tungsten anode X-ray tube (40 kV, 10 mA). The detection system of the experimental setup included an MDR-2 monochromator and a Hamamatsu H8259-01 photon counting device. Measured XRL spectra were corrected for photodetector sensitivity and monochromator transmission. The measurements were performed in reflection geometry at an angle of 90°, i.e. the specimen was placed at 45° to the excitation source and detection channel. The specimens were cooled using a vacuum cryostat.

A.P. Tarasov, A.E. Muslimov, L.A. Zadorozhnaya, V.M. Kanevsky
A.V. Shubnikov Institute of Crystallography, Federal Research Centre Crystallography and Photonics, Russian Academy of Sciences, Leninskii pr. 59, 119333 Moscow, Russia;
e-mail: tarandrew17@gmail.com;
I.D. Venevtsev, P.A. Rodnyi Peter the Great St. Petersburg Polytechnic University, Politekhnicheskaya ul. 29, 195251 St. Petersburg, Russia

Received 16 February 2021
Kvantovaya Elektronika **51** (5) 366–370 (2021)
Translated by O.M. Tsarev

The photoluminescence (PL) of the whiskers was studied at low and high excitation intensities. To obtain PL spectra at low excitation intensity, we used light with a wavelength of 300 nm, spectrally selected in a Cary Eclipse spectrofluorometer equipped with a pulsed xenon lamp (pulse duration, 2 μs; pulse repetition rate, 80 Hz). The power density incident on the sample in this case was estimated at ~0.3 W cm^{-2}. High excitation intensity was provided by the third harmonic (355 nm) of a pulsed Nd:YAG laser (pulse duration, 10 ns; pulse repetition rate, 15 Hz). The incident power density was varied from a few to hundreds of kilowatts per square centimetre. The luminescence of the sample under pulsed laser excitation was detected using an MDR-206 monochromator in combination with a CCD array. The measurements were made at room temperature (RT) and ~80 K.

3. Results and discussion

Figure 1 shows an electron-microscopic image of a ZnO whisker array. The whiskers had a nearly cylindrical shape and were evenly distributed over the substrate surface, but were misaligned. According to electron microscopy data, the whiskers were 40–60 μm in length and 0.5–1 μm in diameter.

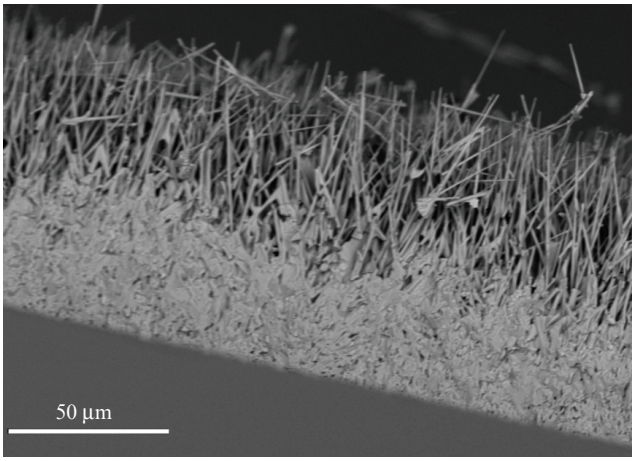

Figure 1. Electron-microscopic image of a ZnO whisker array.

Figure 2 shows low-temperature (~80 K) XRL and PL spectra of the ZnO whisker array under study. The photoluminescence was detected under laser excitation at a power density of 15 kW cm^{-2}. For convenience of interpretation of spectral components, the horizontal axis of the spectra represents energy. Both spectra are seen to have four luminescence bands, denoted as A_i with $i = 1-4$. The bands in the XRL spectrum are located at 3.354, 3.319, 3.244, and 3.175 eV, and those in the PL spectrum, at 3.348, 3.314, 3.237, and 3.168 eV. In addition to the slight difference in band position, probably resulting from the heating of the crystallite surface by the laser beam, the spectra differ in the intensity of bands A_1 and A_2. In particular, the intensity ratio of band A_2 to band A_1 in the PL spectrum is smaller than that in the XRL spectrum.

According to data in the literature, band A_1 corresponds to emission from donor-bound excitons [17, 18]. The strong band at 3.3–3.32 eV (band A_2) is often thought to be the first phonon replica of the free exciton recombination band (FX-LO) [17–19] or originate from surface defects

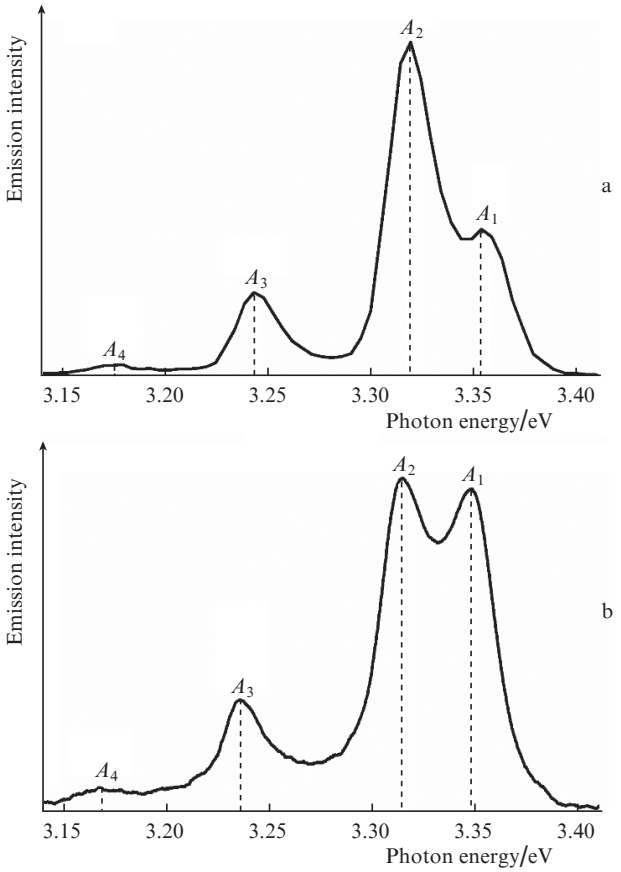

Figure 2. (a) XRL spectrum of the ZnO whisker array and (b) its PL spectrum under laser excitation at a power density of 15 kW cm^{-2}; $T \approx$ 80 K.

[20–22]. To better understand its nature, we compared the spectral shape of this band in ZnO structures differing in the surface-to-volume ratio of their crystallites. Figure 3 shows the PL spectrum of the whisker array and, for comparison, PL spectra, measured under similar conditions, of ZnO nanowalls [23] and ZnO microtetrapods with an arm diameter of ~5 μm, similar to those studied previously [24]. The spectra of all samples are similar in the composition of the bands. For convenience of comparison, the spectra are normalised to the peak intensity of band A_2. It is clearly seen in Fig. 3 that the structures under consideration differ in the intensity ratio of band A_2 to band A_1. It is largest in the spectrum of the nanowalls, which have a large surface area, and smallest in the spectrum of the microrods, where the contribution of the surface is relatively small. Note also the symmetric shape of band A_2, well seen in the PL spectrum of the nanowalls and atypical of phonon replicas of bands [17, 19, 20]. We are thus led to assign band A_2 to surface defects. In the literature, this band is often referred to as A-band [20–22]. The emission in question can be due to transitions involving shallow energy levels of defects [20] or to surface-bound exciton recombination [21, 22]. One possible reason for the higher relative intensity of band A_2 in the XRL spectrum compared to the PL spectrum is that, as a result of the larger penetration depth of X-rays, a considerable contribution to luminescence is made in this case by the polycrystalline layer forming abundantly at the substrate during vapour phase whisker growth without any additional growth catalyst [16, 21, 25]. Structural defects forming on

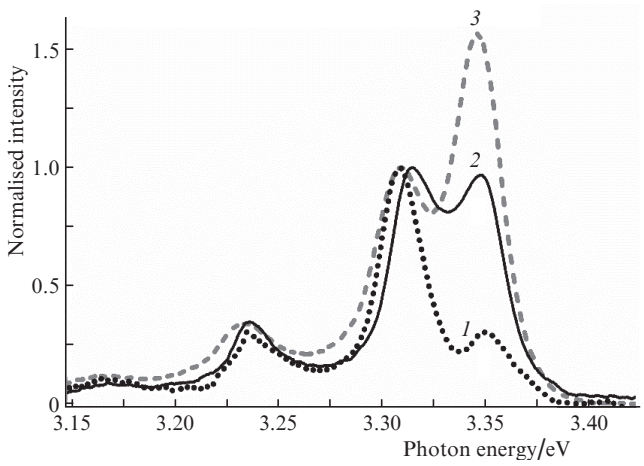

Figure 3. Photoluminescence spectra of ZnO (*1*) nanowalls, (*2*) whiskers, and (*3*) microtetrapods normalised to the peak intensity of band A_2; $T \approx 80$ K.

the surface of crystallites in this layer, e.g. stacking faults [20], can further increase the intensity of band A_2.

Bands A_3 and A_4 are separated from band A_2 by 75 and 144 meV, respectively, which approaches the LO phonon energy in ZnO (72 meV [19, 20]) and twice its value. The correlation of the relative intensities of bands A_3 and A_4 with the intensity of band A_2 in the structures represented in Fig. 3 suggests that these bands are most likely phonon replicas of band A_2.

In addition, we studied the RT luminescent properties of the whisker array. Figure 4a shows the XRL spectrum of the whiskers in the wavelength range 370–640 nm. The NBE luminescence of the sample is represented by a single band, peaking at 386.7 nm. In the visible spectral region, the spectrum contains a broad green luminescence band peaking at about 535 nm, which may comprise several components and be due to transitions involving deep levels of oxygen vacancies in different charge states [26].

Figures 4b and 4c show RT PL spectra of the whiskers at low and high photoexcitation intensities. At the high excitation intensity (laser excitation), the power density incident on the sample was 0.1 MW cm^{-2}. At the low excitation intensity (Fig. 4b), NBE luminescence was represented by a band peaking at 385 nm. At the same time, considerably raising the excitation intensity (Fig. 4c) caused the band to shift to a wavelength of 389.6 nm. Besides, unlike in the case of laser excitation, the spectrum obtained under low-intensity excitation contains a visible luminescence band peaking near 515 nm. Note that the peak position of this band differs from that in the XRL spectrum (Fig. 4a). One possible reason for this is that photons and X-rays differ in penetration depth and, as a consequence, excite different luminescence centres. Even though the NBE emission bands in the XRL and PL spectra differ in position, the shape of the bands and their full width at half maximum (~15 nm) are roughly the same in all three cases represented in Fig. 4.

The shift of the NBE emission band (by about 40 meV in our case) with increasing excitation power is attributable to the formation of an electron–hole plasma (EHP) [27–29]. According to different sources, the density of electron–hole pairs (n_p) necessary for EHP formation (Mott threshold) in ZnO is about 10^{17} to 10^{19} cm^{-3} [30–32]. The n_p produced by optical pumping can be estimated using the relation $n_p = (\rho_{exc}\tau)/(\hbar\omega_{exc} l)$, where ρ_{exc} is the excitation power density; $\hbar\omega_{exc}$ is the excitation photon energy; τ is the electron–hole pair lifetime; and l is the penetration depth of light (~100 nm [32]) or (if electron–hole pair diffusion is taken into account) the diffusion length, which in the case of the nanowhiskers under study can be taken to be equal to their diameter [30]. Taking $\tau = 0.3$ ns [30], we obtain an estimate $n_p \approx 10^{13}$ cm^{-3} in the case of low-intensity excitation and $n_p \approx 10^{18}$ cm^{-3} under laser excitation at $\rho_{exc} = 0.1$ MW cm^{-2}. Thus, at the pulsed laser excitation intensity used, EHP formation in the whiskers at room temperature cannot be ruled out, especially with allowance for the reduced electron–hole interaction in excitons at RT and the mode structure of whisker crystals [30].

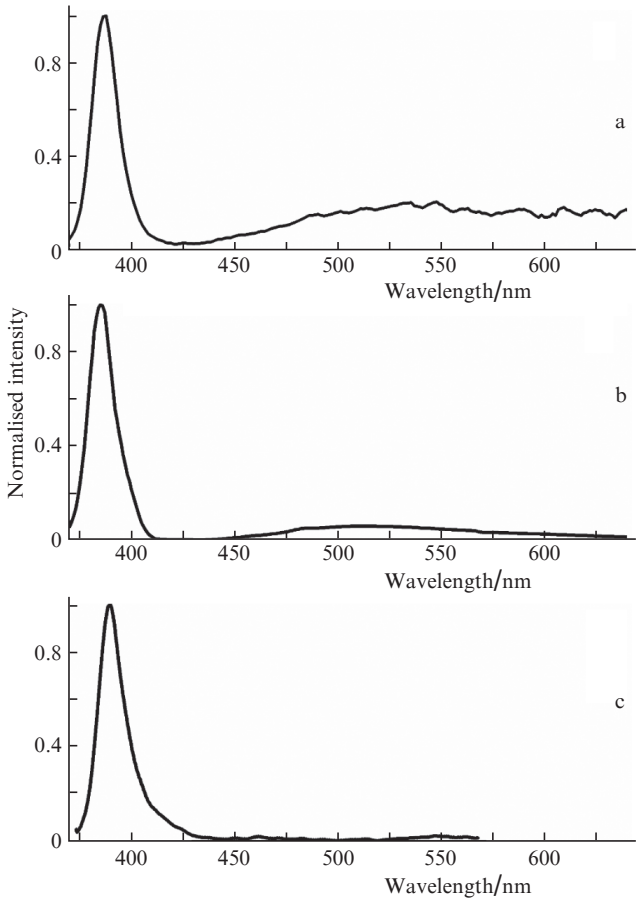

Figure 4. Peak-intensity-normalised (a) XRL, (b) low-excitation-intensity PL, and (c) high-excitation-intensity (0.1 MW cm^{-2}) PL spectra of the ZnO whisker array; $T \approx 300$ K.

To find out the state of carriers in the whiskers under X-ray excitation, we roughly estimate n_p in this case. At a voltage of ~40 kV and a current of 10 mA, the total thermal power is 400 W. The efficiency of a thick-target X-ray tube can be roughly estimated as $\eta = 1.1 \times 10^{-6} ZV$, where Z is the atomic number of the tube target material and V (kV) is the voltage applied to the tube [33]. We used a tungsten target ($Z = 74$) X-ray tube, so we obtain $\eta = 0.0033$ (0.33%), and the X-ray power is ~1.3 W. The zone of the sample under irradiation has the form of a circle ~0.5 cm in diameter. Under the assumption that half (actually, a smaller fraction) of the total power is emitted towards the sample, we obtain a power density of ~6.5 W cm^{-2}. At a linear attenuation coefficient of ~160 cm^{-1} in ZnO (at a photon energy of 20 keV), the volu-

metric density of the absorbed power is 10^3 W cm^{-3}. The power deposited in one whisker about 10^{-11} cm^3 in volume (having a diameter and length of 0.5 and 50 μm, respectively) is then ~10^{-8} W (or ~6×10^{10} eV s^{-1}). Thus, at an average photon energy of 20 keV, about 3×10^6 photons per second are incident on a whisker, i.e. one whisker absorbs on average one X-ray photon in 300 ns. Since this time is considerably longer than the electron–hole pair lifetime in ZnO, we take that all the pairs present in the bulk of a whisker were produced by one X-ray photon.

Thus, to estimate n_p in the case under consideration we should use the energy of one absorbed photon rather than the average volumetric power density. Given that the energy needed for the formation of one pair is about two or three band gaps [34], we find that, at a photon energy of 20 keV, one absorption event leads to the generation of $(2 - 3) \times 10^3$ electron–hole pairs in one crystallite. Finally, knowing the whisker volume we obtain $n_p \approx 10^{14}$ cm^{-3}. It should be noted here that the size of the region over which the pairs have time to spread may be considerably smaller than the crystallite size, but it is very difficult to evaluate even approximately because one has to take into account electron avalanche dynamics and the charge migration length in the thermalisation process. For example, in the case of ionic crystals the size of such a region can be tens to hundreds of nanometres [34, 35], and in some semiconductors the migration length reaches several millimetres [34]. Thus, the above estimate is the lower limit, but it is at least three orders of magnitude below values corresponding to the Mott threshold in ZnO and is of the same order as the estimate in the case of the low-intensity optical excitation used in this study.

Differences in the position and shape of the NBE luminescence band of ZnO crystals under X-ray and low-intensity optical excitation were reported by Ji et al. [14]. The peak position of the XRL band was shifted to longer wavelengths by 110 meV and its width considerably exceeded that in the PL spectrum. Ji et al. [14] assumed that the difference in the position of the band resulted from the fact that different numbers of LO phonons were involved in exciton recombination in the cases of XRL and PL.

In our case, the width of the NBE emission band in the XRL spectrum is essentially the same as in the PL spectra and its shift relative to its position under low-intensity UV excitation is ~15 meV, which is smaller than the LO phonon energy in ZnO. It is reasonable to assume that the shift in the case of XRL is due to luminescence excitation in deeper regions than in the case of PL. As a result, a larger contribution can be made by transitions involving shallow energy levels [36], which will lead to a redshift of the peak position of NBE luminescence.

Thus, comparison of the XRL and PL spectra of the ZnO whisker array demonstrates that, at cryogenic temperatures (~80 K), the general structure of the NBE emission spectrum is the same for both excitation methods and, hence, analysis of XRL with the use of PL data is quite possible. Moreover, the stability of excitons at low temperatures allows pulsed laser excitation to be used at relatively low power densities for observing excitonic optical transitions (Figs 2, 3).

At room temperature, where NBE emission is represented by one, relatively broad, band, distinctions between XRL and PL spectra can be more critical for comparative analysis and unambiguous interpretation of the spectra. Nevertheless, for comparison with XRL it appears more adequate in this case to use PL spectra measured at a low excitation intensity, which produces a similar electron–hole pair density.

4. Conclusions

We have studied luminescent properties of a ZnO whisker array produced by chemical vapour deposition. Two excitation methods have been used: by X-rays and UV radiation. The measurements have been performed at cryogenic (~80 K) and room temperatures. Comparative analysis of the low-temperature XRL and PL spectra of the whiskers has shown that the emission spectra obtained using both excitation methods are similar in structure, which suggests that PL spectroscopy under pulsed laser excitation (at a relatively low power density) can be used in analysis of XRL data. At RT, for comparison with XRL it is more adequate to use PL at a low excitation intensity. However, the distinction between the spectral positions of the NBE luminescence band in XRL and PL spectra can complicate comparative analysis. In our opinion, one possible reason for such a distinction in the case of the whiskers studied here is that X-rays and UV radiation differ in penetration depth and, as a consequence, excite luminescence in different regions.

Acknowledgements. This work was carried out using equipment at the Shared Research Facilities Centre, Federal Research Centre Crystallography and Photonics (FRCCP), Russian Academy of Sciences, and was supported by the RF Ministry of Science and Higher Education (Project No. RFMEFI62119X0035) as part of the state research task for FRCCP (data interpretation), by the Russian Foundation for Basic Research (RFBR) and Rosatom State Corporation as part of Project No. 20-21-00068 (investigation by photoluminescence spectroscopy), and by RFBR as part of Project No. 18-52-76002 ERA-a (investigation by X-ray luminescence spectroscopy).

References

1. Özgür Ü., Hofstetter D., Morkoc H. *Proc. IEEE*, **98**, 1255 (2010).
2. Borysiewicz M.A. *Crystals*, **9**, 505 (2019).
3. Derenzo S.E., Weber M.J., Klintenberg M.K. *Nucl. Instrum. Methods Phys. Res., Sect. A*, **486**, 214 (2002).
4. Simpson P.J., Tjossem R., Hunt A.W., Lynn K.G., Munné V. *Nucl. Instrum. Methods Phys. Res., Sect. A*, **505**, 82 (2003).
5. Gorokhova E.I., Rodnyi P.A., Khodyuk I.V., Anan'eva G.V., Demidenko V.A., Bourret-Courchesne E.D. *J. Opt. Technol.*, **75**, 741 (2008) [*Opt. Zh.*, **75**, 66 (2008)].
6. Bourret-Courchesne E.D., Derenzo S.E., Weber M.J. *Nucl. Instrum. Methods Phys. Res., Sect. A*, **601**, 358 (2009).
7. Turtos R.M., Gundacker S., Lucchini M.T., Procházková L., Čuba V., Burešová H., Mrázek J., Nikl M., Lecoq P., Auffray E. *Phys. Status Solidi RRL*, **10**, 843 (2016).
8. Yanagida T. *Proc. Jpn. Acad., Ser. B*, **94**, 75 (2018).
9. Dorenbos P. *IEEE Trans. Nucl. Sci.*, **57**, 1162 (2010).
10. Lecoq P. *Nucl. Instrum. Methods Phys. Res., Sect. A*, **809**, 130 (2016).
11. Armelao L., Heigl F., Jürgensen A., Blyth R.I.R., Regier T., Zhou X.T., Sham T.K. *J. Phys. Chem. C*, **111**, 10194 (2007).
12. Li Q., Liu X., Gu M., Hu Y., Li F., Liu S., Wu Q., Sun Z., Zhang J., Huang S., Zhang Z., Zhao J. *Opt. Express*, **26**, 31290 (2018).
13. Angub M.C.M., Vergara C.J.T., Husay H.A.F., Salvador A.A., Empizo M.J.F., Kawano K., Minamic Y., Shimizuc T., Sarukura N., Somintac A.S. *J. Lumin.*, **203**, 427 (2018).
14. Ji J., Colosimo A.M., Anwand W., Boatner L.A., Wagner A., Stepanov P.S., Trinh T.T., Liedke M.O., Krause-Rehberg R., Cowan T.E., Selim F.A. *Sci. Rep.*, **6**, 1 (2016).

15. Crapanzano R., Villa I., Mostoni S., D'Arienzo M., Di Credico B., Fasoli M., Scotti R., Vedda A. *Nanomaterials*, **10**, 1983 (2020).
16. Red'kin A.N., Makovei Z.I., Gruzintsev A.N., Yakimov E.E., Kononenko O.V., Firsov A.A. *Inorg. Mater*., **45**, 1246 (2009) [*Neorg. Mater*., **45**, 1330 (2009)].
17. Foreman J.V., Simmons J.G., Baughman W.E., Liu J., Everitt J.O. *J. Appl. Phys.*, **113**, 133513 (2013).
18. Cao W., Du W. *J. Lumin*., **124**, 260 (2007).
19. Wang L., Giles N.C. *J. Appl. Phys*., **94**, 973 (2003).
20. Tainoff D., Masenelli B., Mélinon P., Belsky A., Ledoux G., Amans D., Dujardin C., Fedorov N., Martin P. *Phys. Rev. B*, **81**, 115304 (2010).
21. Bekeny C., Voss T., Hilker B., Gutowski J., Hauschild R., Kalt H., Postels B., Bakin A., Waag A. *J. Appl. Phys*., **102** (4), 044908 (2007).
22. Fallert J., Hauschild R., Stelzl F., Urban A., Wissinger M., Zhou H., Klingshirn C., Kalt H. *J. Appl. Phys*., **101**, 073506 (2007).
23. Tarasov A.P., Briskina C.M., Markushev V.M., Zadorozhnaya L.A., Volchkov I.S. *Opt. Mater*., **102**, 109823 (2020).
24. Tarasov A.P., Briskina Ch.M., Markushev V.M., Zadorozhnaya L.A., Lavrikov A.S., Kanevsky V.M. *JETP Lett*., **110**, 739 (2019) [*Pis'ma Zh. Eksp. Teor. Fiz.*, **110**, 750 (2019)].
25. Plakhova T.V., Shestakov M.V., Baranov A.N. *Inorg. Mater.*, **48**, 469 (2012) [*Neorg. Mater*., **48**, 549 (2012)].
26. Muslimov A.E., Venevtsev I.D., Zadorozhnaya L.A., Rodnyi P.A., Kanevsky V.M. *JETP Lett*., **112**, 225 (2020) [*Pis'ma Zh. Eksp. Teor. Fiz.*, **112**, 240 (2020)].
27. Bagnall D.M., Chen Y.F., Shen M.Y., Zhu Z., Goto T., Yao T. *J. Cryst. Growth*, **184**, 605 (1998).
28. Yamamoto A., Kido T., Goto T., Chen Y., Yao T. *Solid State Commun*., **122**, 29 (2002).
29. Klini A., Androulidaki M., Anglos D. *Sensors*, **19**, 5490 (2019).
30. Klingshirn C., Hauschild R., Fallert J., Kalt H. *Phys. Rev. B*, **75**, 1 (2007).
31. Versteegh M.A., Kuis T., Stoof H.T.C., Dijkhuis J.I. *Phys. Rev. B*, **84**, 035207 (2011).
32. Özgür Ü., Alivov Y.I., Liu C., Teke A., Reshchikov M., Doğan S., Avrutin V., Cho S.-J., Morkoç A.H. *J. Appl. Phys*., **98**, 11 (2005).
33. McCall G.H. *J. Phys. D: Appl. Phys*., **15**, 823 (1982).
34. Rodnyi P.A. *Physical Processes in Inorganic Scintillators* (Boca Raton: CRC Press LLC, 1997).
35. Belsky A., Ivanovskikh K., Vasil'ev F., Joubert M.F., Dujardin C. *J. Phys. Chem. Lett*., **4**, 3534 (2013).
36. Srikant V., Clarke D.R. *J. Appl. Phys*., **83**, 5447 (1998).